Supporting Information

A heterocycle fusing strategy for simple construction of efficient solution-processable pure-red thermally activated delayed fluorescence emitters

Xu Gong [a, c], Yepeng Xiang [a], Weimin Ning [a], Lisi Zhan [a], Shaolong Gong [a, c, *], Guohua Xie [a, *], Chuluo Yang [a, b*]

[a] *Department of Chemistry, Hubei Key Lab on Organic and Polymeric Optoelectronic Materials, Renmin Hospital of Wuhan University, Wuhan University, Wuhan 430072, China*

[b] *Shenzhen Key Laboratory of New Information Display and Storage Materials，College of Materials Science and Engineering, Shenzhen University, Shenzhen 518060, China.*

[c] *Shenzhen Research Institute of Wuhan University, Wuhan University, Shenzhen 518057, China*

E-mail address:

(S.G.) E-mail: slgong@whu.edu.cn
(G.X.) E-mail: guohua.xie@whu.edu.cn
(C.Y) E-mail: clyang@whu.edu.cn

Materials and instrument:

All reagents were used as received from commercial sources unless otherwise stated. Tetrahydrofuran and toluene were dried by sodium-potassium alloy. ^{1}H NMR NMR spectra were measured on a Bruker Advanced II (400 MHz) spectrometers or MERCURYVX300. High-resolution mass spectra (HRMS) were measured on a LCQ-Orbitrap Elite (Thermo-Fisher Scientific, Waltham, MA, USA) mass spectrometer. The glass transition temperature (T_g) was determined from the second heating scan. Thermogravimetric analysis (TGA) was undertaken with a NETZSCH STA 449C instrument. The thermal stability of the samples under a nitrogen atmosphere was determined by measuring their weight loss while heating at a rate of 10 ^{o}C min^{-1} from 25 to 600 ^{o}C. Cyclic voltammetry (CV) was carried out in nitrogen-purged trichloromethane or tetrahydrofuran at room temperature with a CHI voltammetric analyser. Tetrabutylammonium hexafluorophosphate ($TBAPF_6$) (0.1 M) was used as the supporting electrolyte. The conventional three-electrode configuration consists of a platinum working electrode, a platinum wire auxiliary electrode, and an Ag wire pseudo-reference electrode with ferrocenium–ferrocene (Fc^{+}/Fc) as the internal standard. Cyclic voltammograms were obtained at a scan rate of 100 mV s^{-1}. Formal potentials are calculated as the average of cyclic voltammetric anodic and cathodic peaks. The measurement of atomic force microscope (AFM) was carried out with a Cypher ES, Asylum Research, USA. UV-vis absorption spectra were obtained with a Shimadzu UV-3600 UV-vis-NIR spectrometer. The steady-state photoluminescence spectra were recorded on a Hitachi F-4600 fluorescence spectrophotometer. The

transient photoluminescence (PL) spectra were measured by a single photon counting spectrometer from Edinburgh Instruments (FLS920) with a Picosecond Pulsed UV-LASTER (LASTER377) as the excitation source. The absolute photoluminescence quantum yields (PLQYs) were obtained using a Quantaurus-QY measurement system (C9920-02, Hamamatsu Photonics) and all the samples were excited at 300 nm. Current density-voltage characteristics, luminance and the EL spectra were recorded with a Keithley 2400 source meter unit and a Photoresearch SpectraScan PR735 spectrometer. The EQE was calculated from the current density, luminance and EL spectrum, assuming a Lambertian distribution. Ground state structures and FMOs were obtained by B3LYP density functional method with basis set def2-SVP. The dispersion correction was conducted by Grimme's D3 version with BJ damping function. Time-dependent DFT with PBE0 functional and basis set def2-SVP were then performed to further analyze the excited states with the optimized ground state structures.

Device fabrication and characterization:

The prepatterned indium tin oxide (ITO) substrates were cleaned by ultrasonic acetone bath, followed by ethanol bath. Afterward, the substrates were dried with N_2 and then loaded into a UV-ozone chamber. After UV-Ozone treatment, the m-PEDOT:PSS layer was spin-coated on the ITO substrate at 4000 rpm as the hole-injecting layer. The substrate was transferred into a N_2 filled glove box and then annealed at 120 °C for 10 mins to remove the residual solvent. The emissive layer was prepared by spin-coating directly on the hole-injecting layer at 1000 rpm, and then annealed at 50 °C for 10 mins. The electron-transporting material, the electron injecting materials and the cathode

materials were consecutively evaporated in a vacuum chamber under 10^{-5} mbar. Before being taken out of the glovebox, the devices were encapsulated with UV-curable epoxy. The voltage-current-luminance characteristics and the electroluminescence (EL) spectra were simultaneously measured with PR735 SpectraScan Photometer and Keithley 2400 sourcemeter unit under ambient atmosphere at room temperature. The EQE was calculated from the current density, luminance and EL spectrum, assuming a Lambertian distribution.

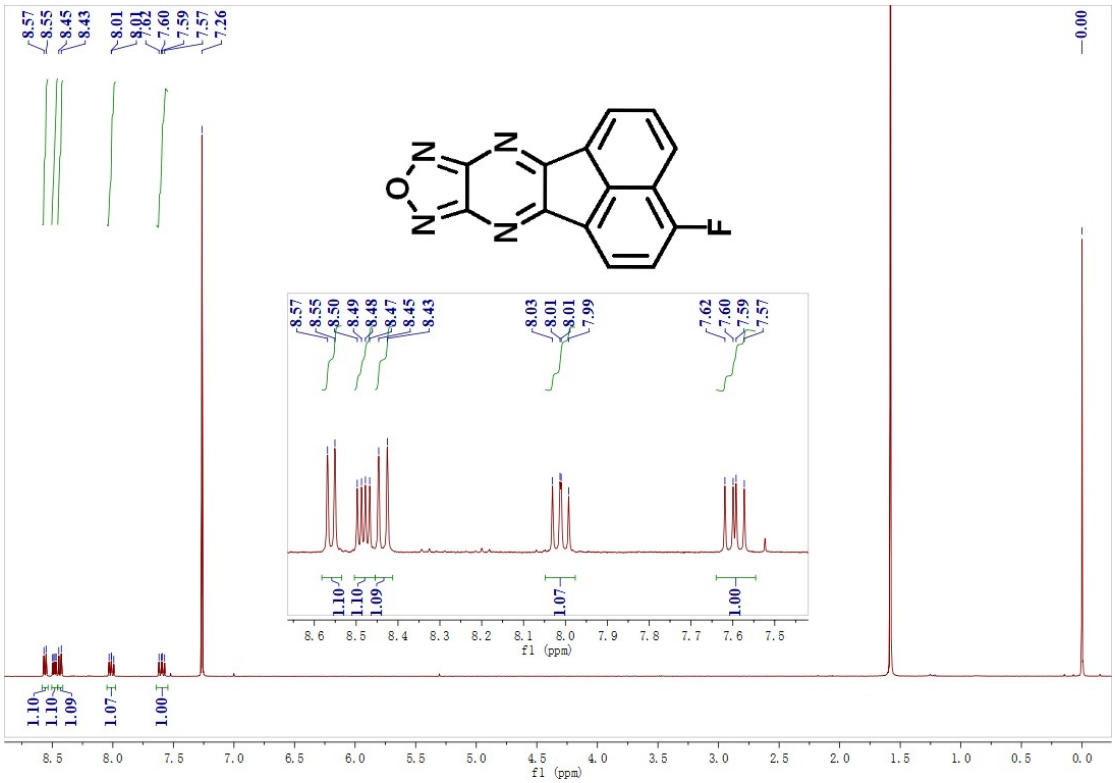

Figure S1. ^{1}H NMR spectrum of ANOP-F (400 MHz, $CDCl_3$ + TMS, 300 K).)

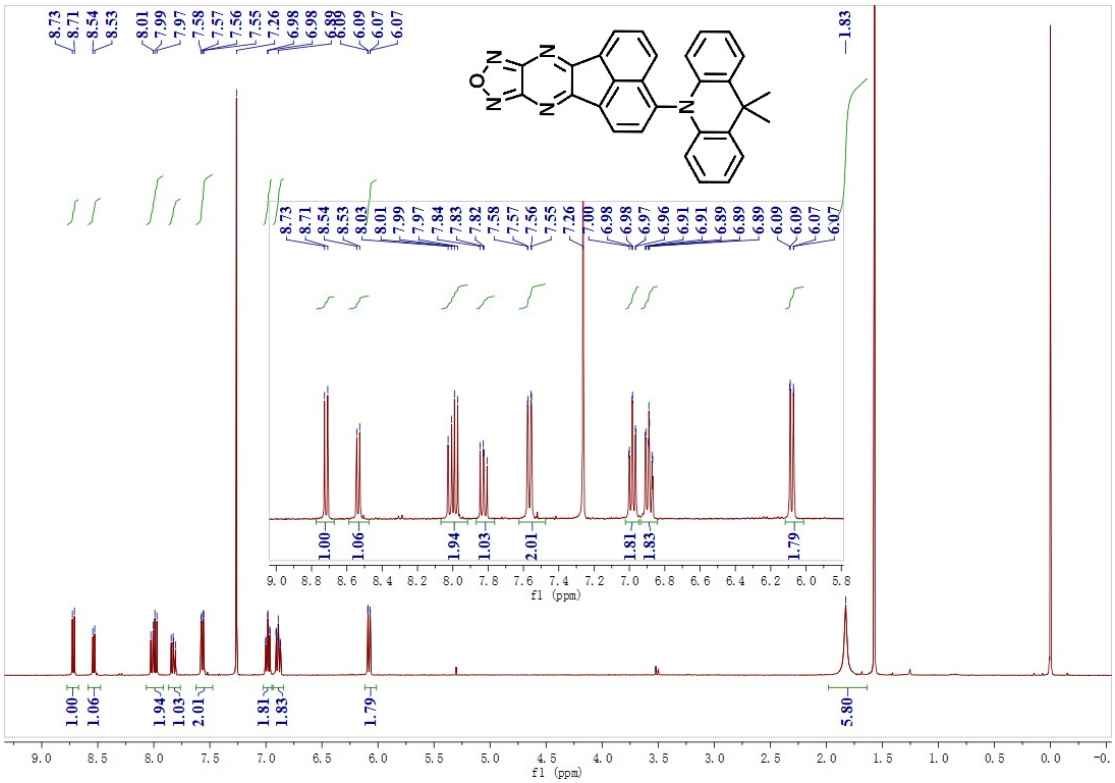

Figure S2. ^{1}H NMR spectrum of ANOP-DMAC (400 MHz, $CDCl_3$ + TMS, 300 K).)

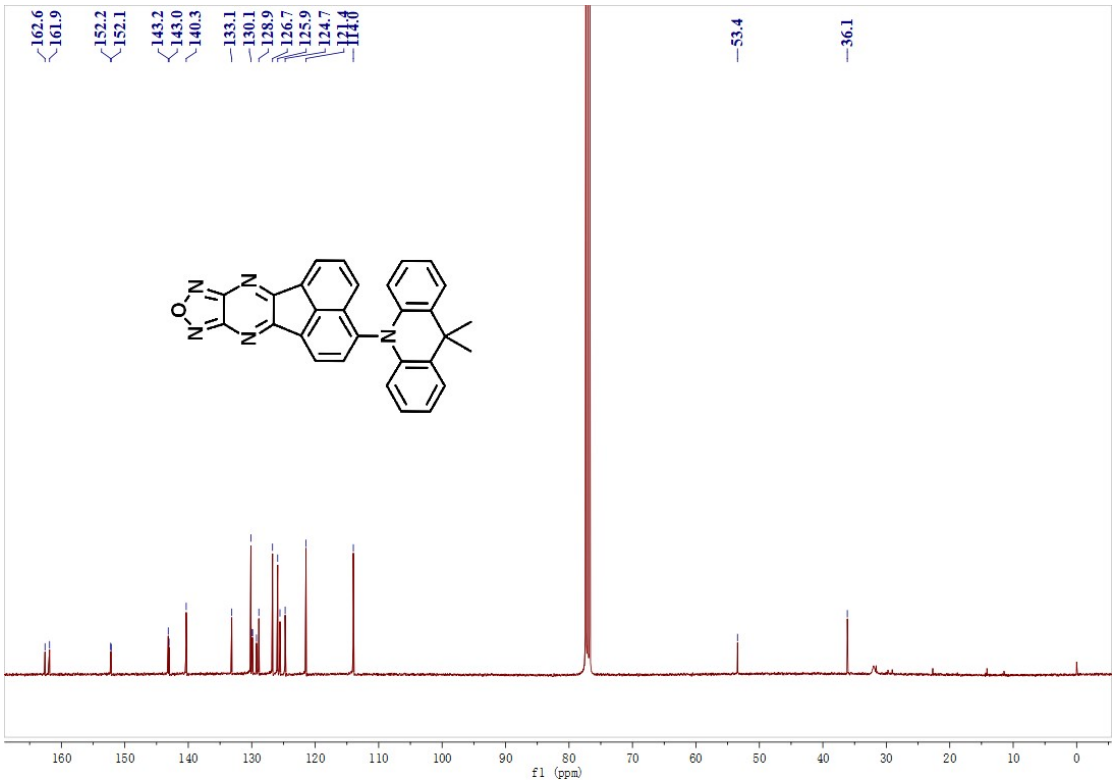

Figure S3. ^{13}C NMR spectrum of ANOP-DMAC (100 MHz, $CDCl_3$ + TMS, 300 K).)

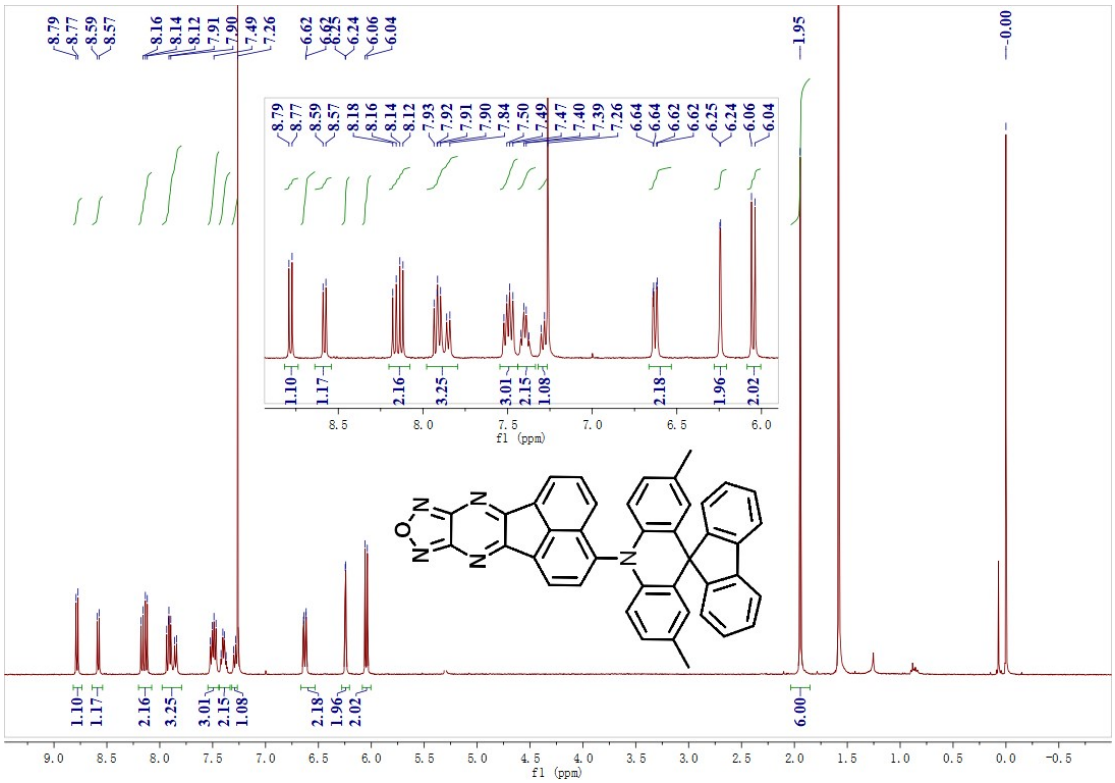

Figure S4. ^{1}H NMR spectrum of ANOP-MeFAC (400 MHz, $CDCl_3$ + TMS, 300 K).)

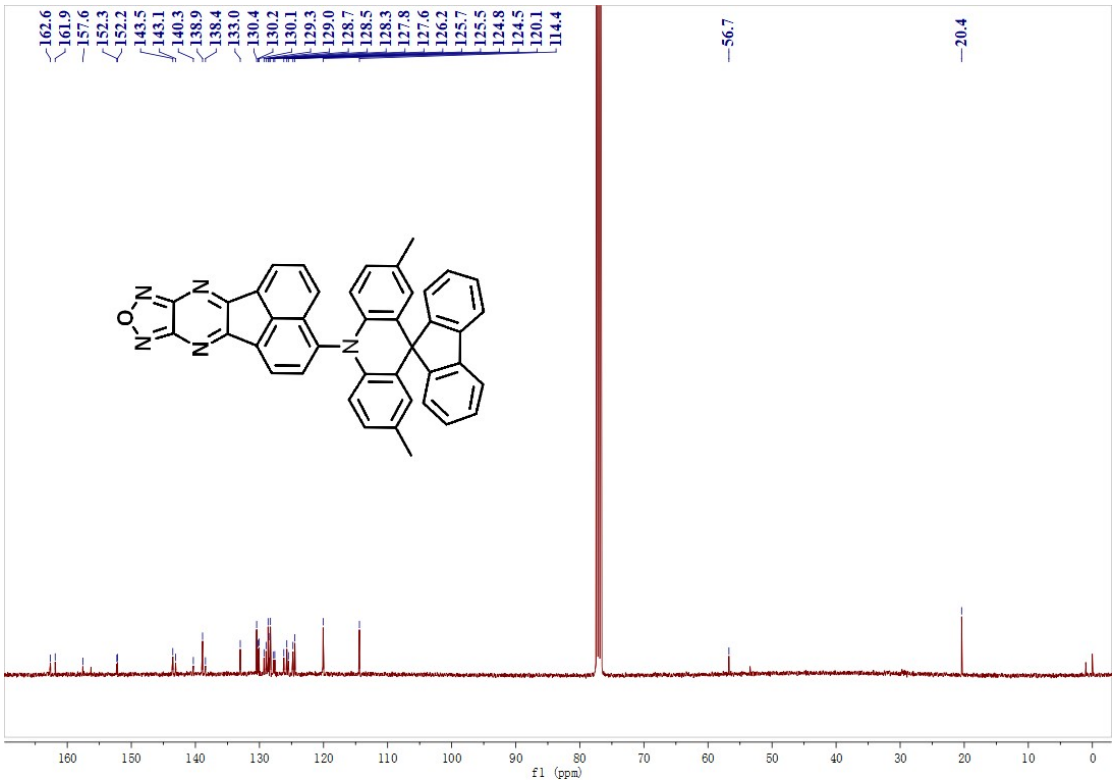

Figure S5. ^{13}C NMR spectrum of ANOP-MeFAC (100 MHz, $CDCl_3$ + TMS, 300 K).)

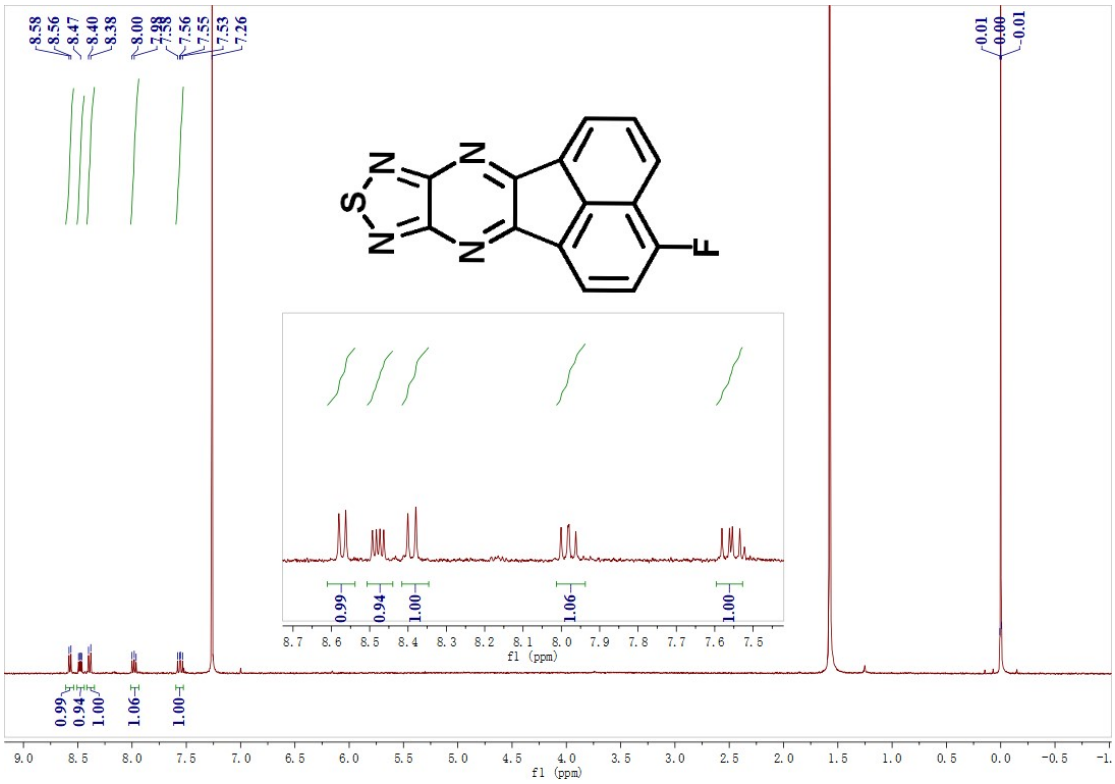

Figure S6. ^{1}H NMR spectrum of ANTP-F (400 MHz, $CDCl_3$ + TMS, 300 K).)

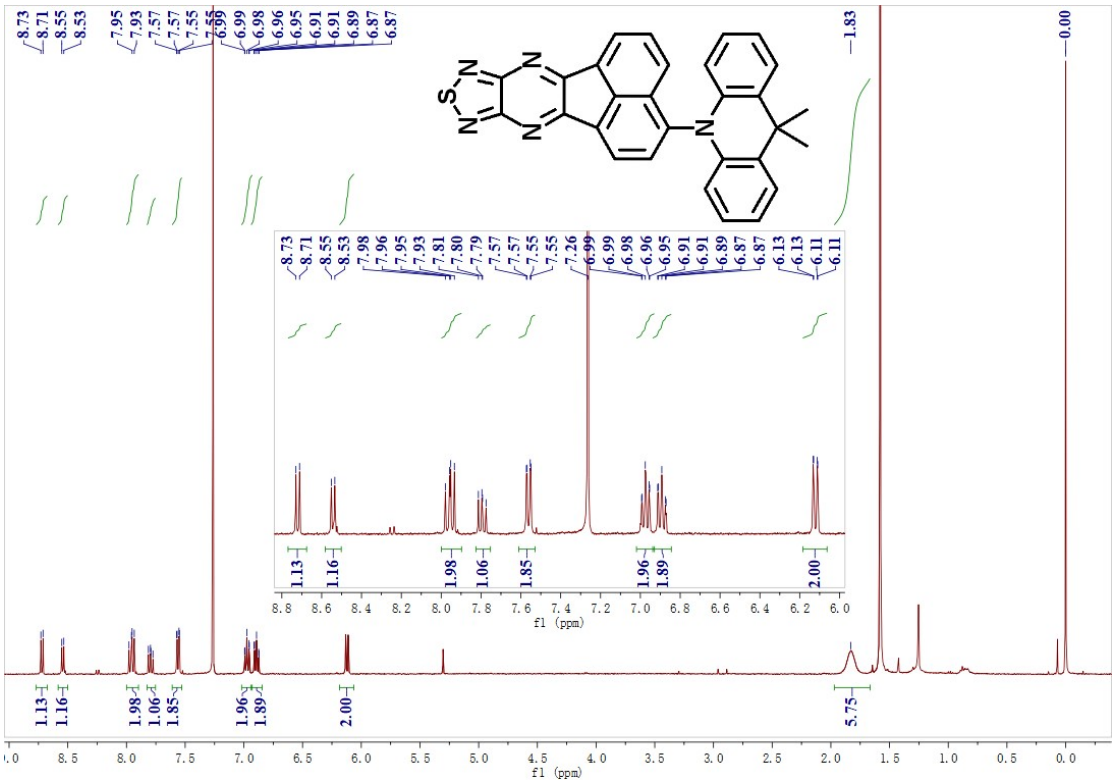

Figure S7. ^{1}H NMR spectrum of ANTP-DMAC (400 MHz, $CDCl_3$ + TMS, 300 K).)

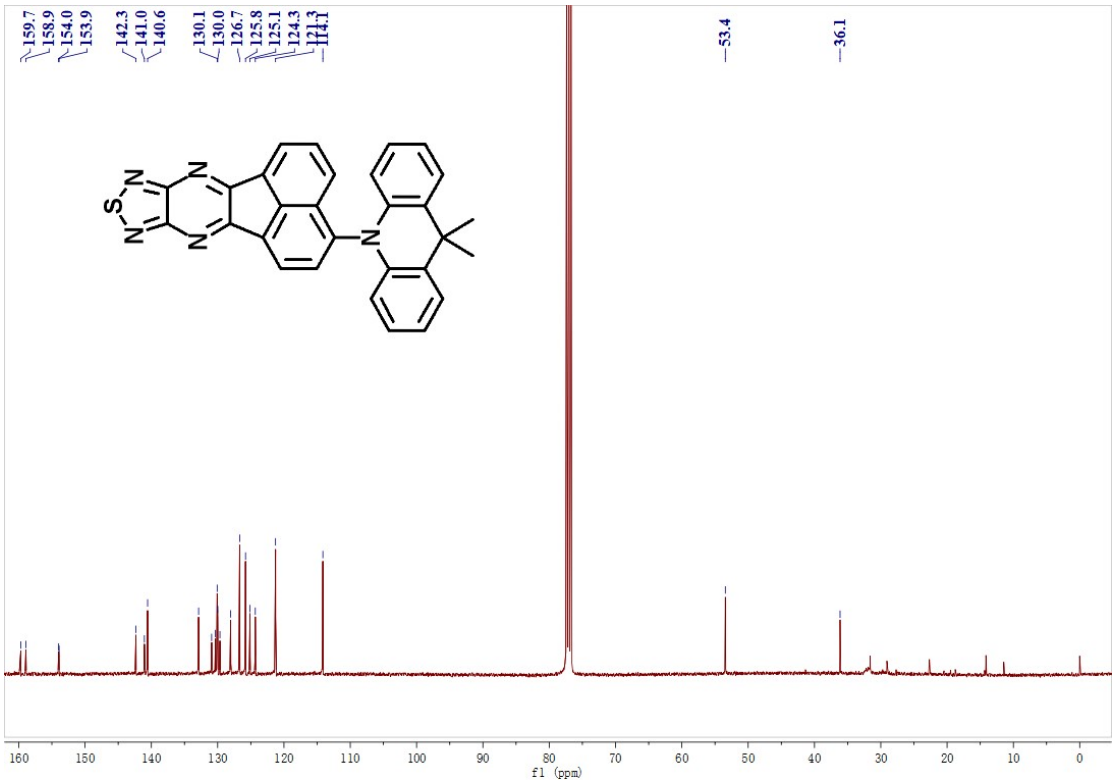

Figure S8. ^{13}C NMR spectrum of ANTP-DMAC (100 MHz, $CDCl_3$ + TMS, 300 K).)

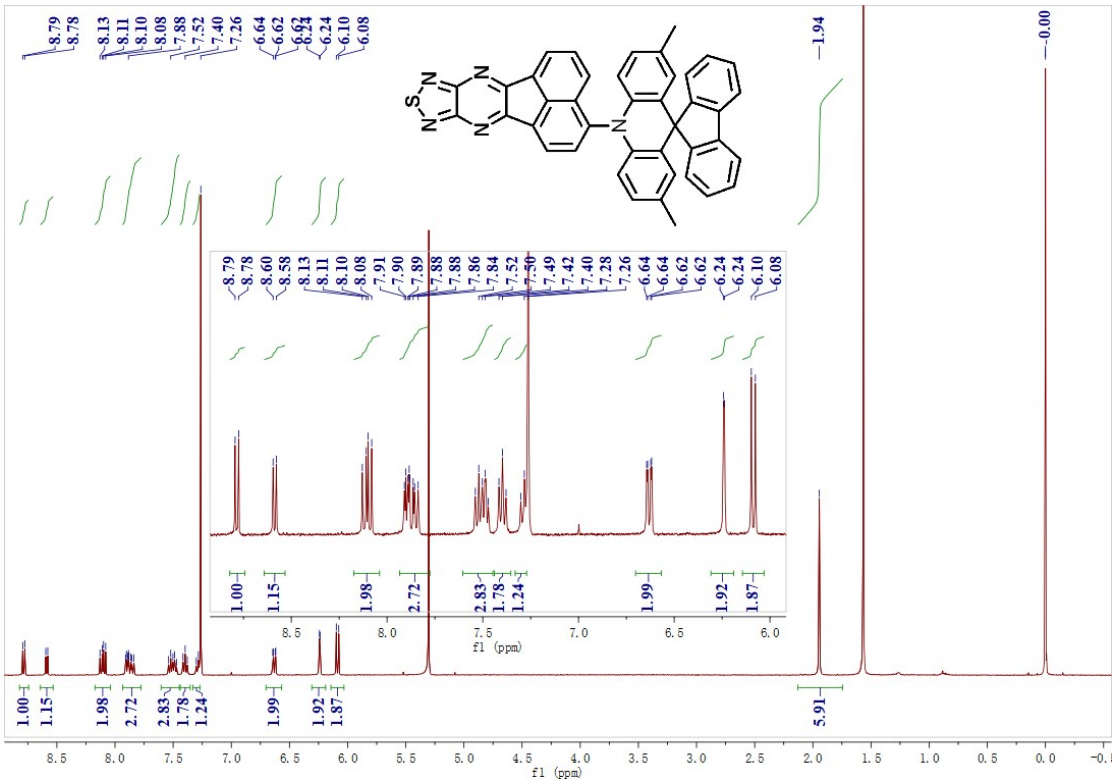

Figure S9. ^{1}H NMR spectrum of ANTP-MeFAC (400 MHz, $CDCl_3$ + TMS, 300 K).)

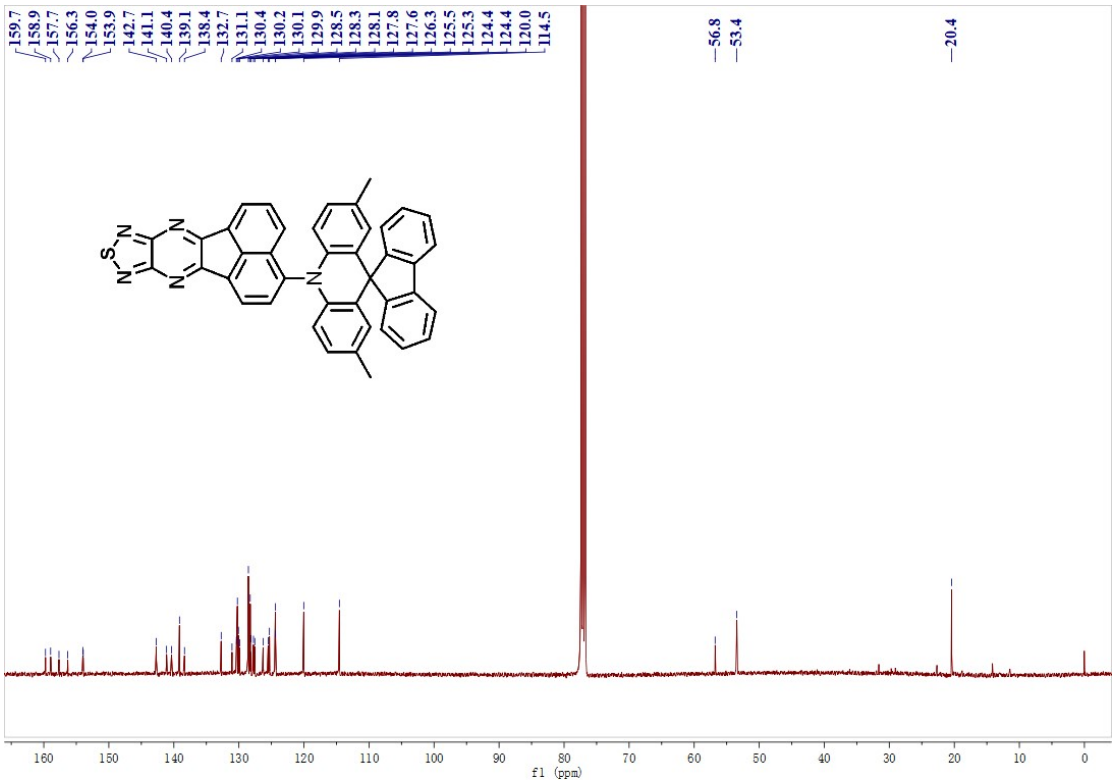

Figure S10. ^{13}C NMR spectrum of ANTP-MeFAC (100 MHz, $CDCl_3$ + TMS, 300 K).)

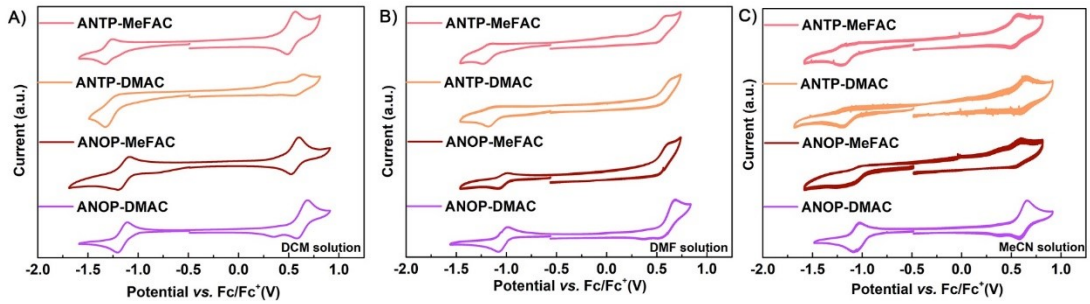

Figure S11. Cyclic voltammograms of all the emitters in different solvents.

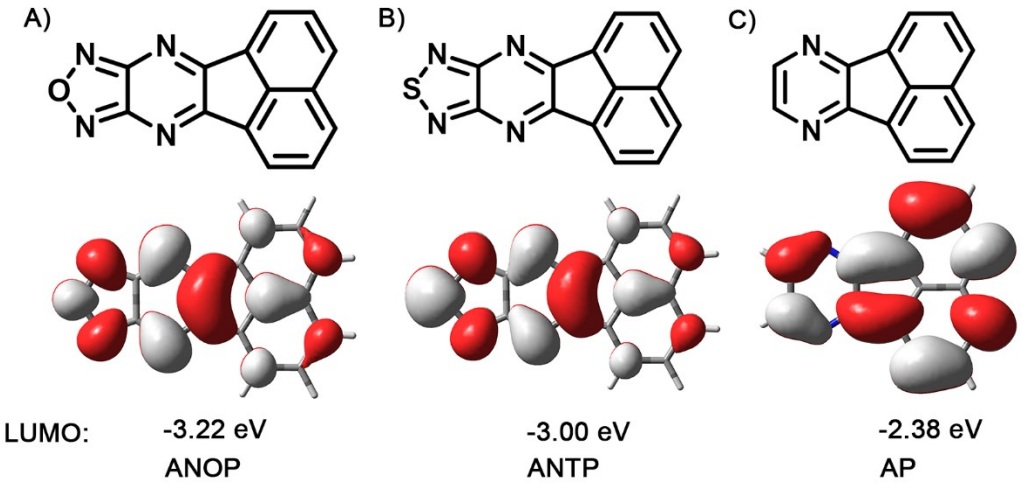

Figure S12. Chemical structures of acceptors, their LUMO distributions, and corresponding energy levels.

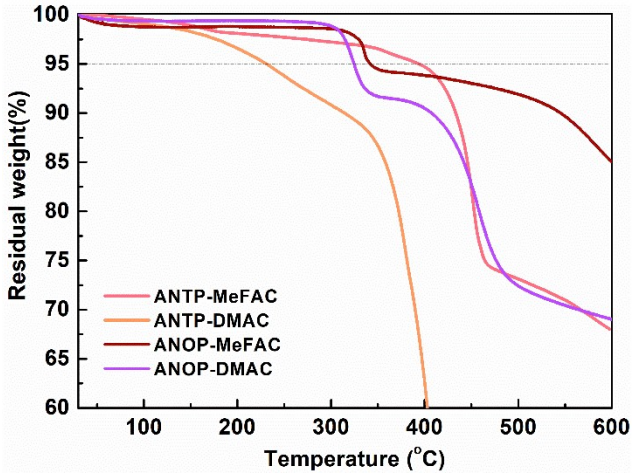

Figure S13. TGA traces of TADF emitters recorded at a heating rate of 10 °C min^{-1}.

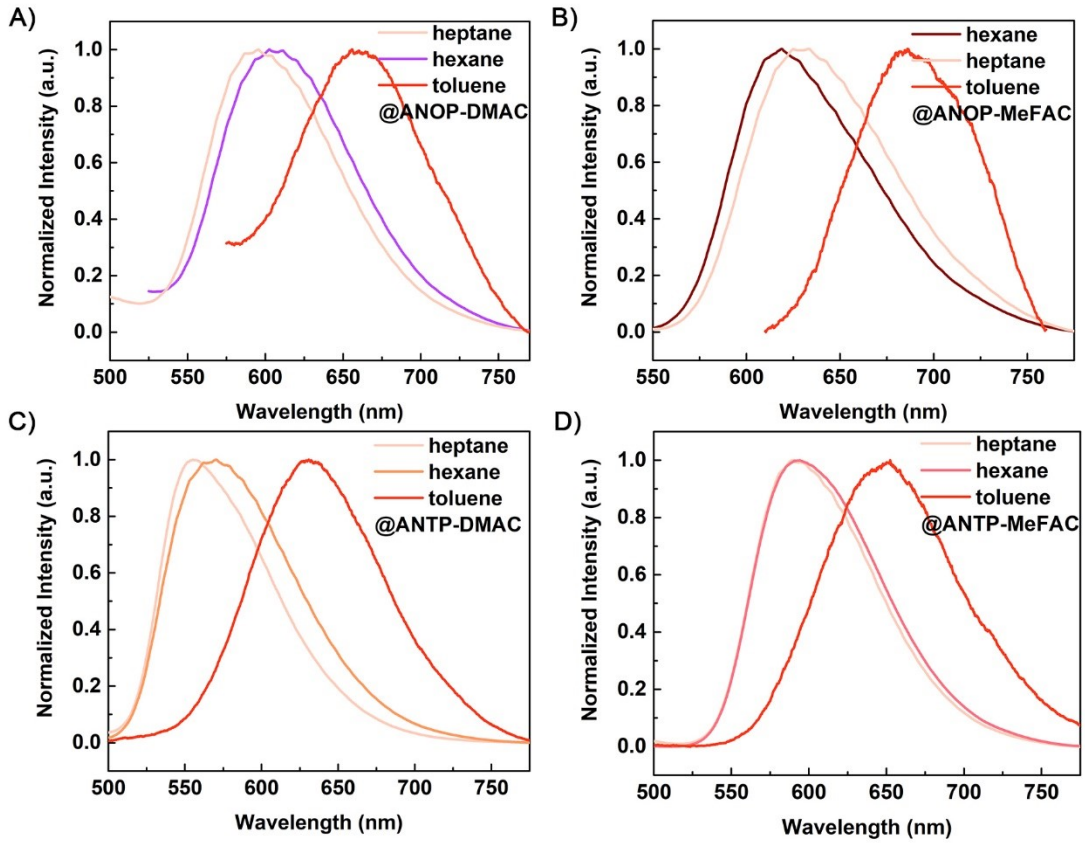

Figure S14. The PL spectra of A) ANOP-DMAC, B) ANOP-MeFAC, C) ANTP-DMAC, and D) ANTP-MeFAC in various solvents (10^{-5} M).

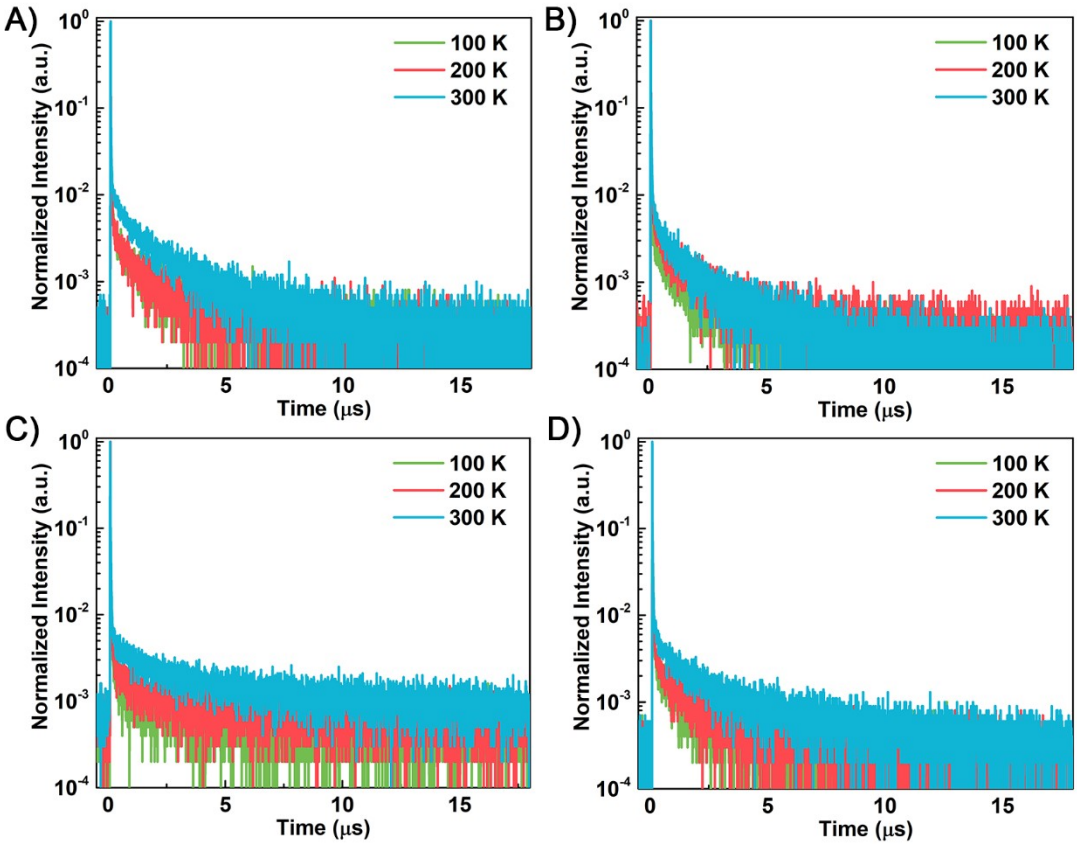

Figure S15. Transient PL curves of 5 wt% ANOP-DMAC A), ANOP-MeFAC B), ANTP-DMAC C) and ANTP-MeFAC doped in mCP host.

Table S1. The physical properties of ANXP series.

Compounds	HOMO[a)] [eV]	LUMO[a)] [eV]	RMS [b)] [nm]	TGA [c)] [°C]
ANOP-DMAC	-5.48/-5.41/-5.41/-5.43	-3.64/-3.76/-3.75/-3.72	0.374	325
ANOP-MeFAC	-5.36/-5.37/-5.35/-5.36	-3.65/-3.77/-3.71/-3.71	0.261	342
ANTP-DMAC	-5.40/-5.32/-5.40/-5.37	-3.56/-3.67/-3.63/-3.62	0.355	231
ANTP-MeFAC	-5.33/-5.29/-5.34/-5.32	-3.51/-3.62/-3.61/-3.58	0.275	394

[a] Obtained from Cyclic voltammograms in CH_2Cl_2, DMF and MeCN solution at room temperature and the average data, respectively. [b] Measured in mCP host films with a doping concentration of 5wt%.

Table S2. The photophysical properties of ANXP series in hexane solution.

Compounds	λ_{PL} [a)] [nm]	λ_{abs} [a)] [nm]	$\tau_p/\tau_d/r_d$ [a)] [ns]/ [μs]/ [%]
ANOP-DMAC	571	310, 370, 500	6.6/5.6/31
ANOP-MeFAC	606	310, 371, 531	12.4/3.1/40
ANTP-DMAC	546	326, 355, 477	6.7/7.2/17
ANTP-MeFAC	580	326, 356, 534	9.8/12.9/79

[a]Measured in diluted hexane solutions (10^{-5} M) at room temperature.

Table S3. The rate constants for 5 wt % TADF emitters doped into the mCP host.

Emitter	k_r [10^6 s^{-1}]	k_{RISC} [10^5 s^{-1}]	k_{nr} [10^7 s^{-1}]	k_r/k_{nr}
ANOP-DMAC	4.5	8.0	2.6	0.17
ANOP-MeFAC	4.4	11.2	2.2	0.20
ANTP-DMAC	9.7	6.5	0.83	1.2
ANTP-MeFAC	5.8	10.1	0.56	1.0

Table S4. The summary of TADF-OLED characteristics from reported emitters with similar emissions in literatures. Device data are taken from Ref.

Compound	V_{on} [V]	CE_{max} [cd/A]	PE_{max} [lm/W]	EQE_{max} [%]	EL_{peak} [nm]	CIE [x, y]	Ref.
ANOP-DMAC	**7**	**1.9**	**0.67**	**4.4**	**672**	**0.62, 0.34**	**-**
ANOP-MeFAC	**8**	**1.5**	**0.48**	**3.5**	**668**	**0.61, 0.34**	**-**
ANTP-DMAC	**6**	**8.0**	**2.8**	**6.8**	**630**	**0.59, 0.40**	**-**
ANTP-MeFAC	**6**	**5.9**	**2.1**	**6.1**	**640**	**0.61, 0.38**	**-**
DDTPACz_DCPP_10 %	4.8	13.6	9	13.6	646	0.61, 0.38	[1]
B4	-	1.5	1.1	1.4	636	0.60, 0.38	[2]
B5	-	1	0.61	1.2	648	0.63, 0.37	[2]
HATNA-tCz_5	-	0.93	0.27	1.8	668	0.65, 0.34	[3]
B7	-	0.46	0.24	0.91	670	0.64, 0.36	[2]
HATNA-tCz_10	-	0.34	0.1	1.2	682	0.68, 0.32	[3]
HATNA-tPCz_5	-	1.54	0.54	4.8	692	0.66, 0.32	[3]
MPPA-MCBP	5.1	-	-	0.62	698	0.67, 0.31	[4]
MPPA: MCBP	5.8	-	-	0.11	710	0.69, 0.31	[4]
MPPA-3Cz	6.2	-	-	0.25	715	0.69, 0.30	[5]
BDFCA		-	-	9.69	721	-	[6]
MPPA-Cz	6.4	-	-	0.06	728	0.70, 0.29	[5]

Reference

[1] B. Wang, H. Yang, Y. Zhang, G. Xie, H. Ran, T. Wang, Q. Fu, Y. Ren, N. Sun, G. Zhao, J.-Y. Hu, Q. Wang, *J. Mater. Chem. C* **2019**, 7, 12321.

[2] Y. Wang, Y. Zhu, G. Xie, Q. Xue, C. Tao, Y. Le, H. Zhan, Y. Cheng, *Org. Electron.* **2018**, 59, 406.

[3] X. Zhou, Y. Xiang, S. Gong, Z. Chen, F. Ni, G. Xie, C. Yang, *Chem Commun* **2019**, 55, 14190.

[4] K. Sun, Y. Sun, D. Liu, Y. Feng, X. Zhang, Y. Sun, W. Jiang, *Dye Pigm.* **2017**, 147, 436.

[5] K. Sun, D. Chu, Y. Cui, W. Tian, Y. Sun, W. Jiang, *Org. Electron.* **2017**, 48, 389.

[6] D.-H. Kim, A. D'Aléo, X.-K. Chen, A. D. S. Sandanayaka, D. Yao, L. Zhao, T. Komino, E. Zaborova, G. Canard, Y. Tsuchiya, E. Choi, J. W. Wu, F. Fages, J.-L. Brédas, J.-C. Ribierre, C. Adachi, *Nat. Photonics* **2018**, 12, 98.